

## Electroconvection in nematic liquid crystals in Hele-Shaw cells

Jong-Hoon Huh

*Department of Mechanical Systems Engineering, Faculty of Computer Science and Systems Engineering, Kyushu Institute of Technology, Fukuoka 820-8502, Japan*

Shoichi Kai

*Department of Applied Physics and Graduate School of Systems Life Science, Faculty of Engineering, Kyushu University, Fukuoka 812-8581, Japan*

(Received 10 April 2003; published 23 October 2003)

We report electrohydrodynamic instability in nematic liquid crystals found in Hele-Shaw cells. Due to the present cell geometry, the convective structures could be directly visualized as surface or bulk flows. An unexpected structure is observed, which is completely different from the well-known patterns in the standard cells. By using the voltage-frequency jump method, the stability of a convective structure in Hele-Shaw cells is discussed in terms of the Busse diagram.

DOI: 10.1103/PhysRevE.68.042702

PACS number(s): 61.30.-v, 47.20.Lz

One of many attractive examples of pattern-forming physics describing dissipative structures out of equilibrium [1,2] is ac-driven electroconvection (EC) in liquid crystals. It provides us with a rich variety of patterns that are fundamentally related with the anisotropy of liquid crystals. The primary EC pattern, the Williams domain (WD), at a threshold field appears due to the so-called Carr-Helfrich mechanism [3]. Increasing the electric field and changing its frequency, one also observes various secondary instabilities such as the zigzag instability, the Eckhaus instability, the abnormal roll instability, and so on [4–7]. For the last three decades EC has been intensively studied experimentally and theoretically, and could be understood more systematically. However, there still remain many questions related to various pattern formations in electrohydrodynamic instability. In this report we address EC in nematic liquid crystals in Hele-Shaw cells [8] in which we can directly observe full convective structures; the standard patterns such as the WD, the dynamic scattering mode (DSM) below a critical frequency  $f_c$ , and the chevron pattern above  $f_c$  [9,10]. In addition to these, a sawteethlike pattern that was not expected before has been observed. We have investigated the stability problem of the dissipative structure in terms of the Busse diagram [4,11].

We have prepared Hele-Shaw cells, as shown in Fig. 1. The thickness  $r$  of nematic films between two slide glasses was safely maintained with electrodes. We have used a commercial aluminum foil ( $r=12\ \mu\text{m}$ ) or a micropolished stainless cutter ( $r=180\ \mu\text{m}$ ) as the electrodes. The gap  $d$  between two electrodes was set in  $d=200\ \mu\text{m}$ ,  $500\ \mu\text{m}$ , and  $1000\ \mu\text{m}$ . The dimension of nematic films in the  $x$  direction was sufficiently large ( $\sim 26\ \text{mm}$ ). In order to achieve the planar alignment, we carried out the rubbing treatment along the  $x$  direction parallel to the glasses. A well-known nematic liquid crystal, MBBA (*p*-methoxybenzilidene-*p'*-*n*-butylaniline) was used in the present study. Moreover, in order to observe the flow of electroconvection, small particles [micropearl (Sekisui Chemical) of diameter  $3.88\ \mu\text{m}$ ] were mixed with the liquid crystal [12]. Across these cells was applied an alternating electric field  $E = E_0 \cos(2\pi ft)$  [ $\vec{E}$

$= (0, 0, \pm E_z)$ ], which was generated by a function synthesizer (NF-1915) and an amplifier (F20A, Toyo Tech). The function synthesizer was controlled via the standard general purpose interface bus (GPIB) by a computer. At room temperature, the electroconvection patterns were observed in the  $xz$  plane (side-view) parallel to the electrodes by use of a charge-coupled device (SONY XC-75) mounted on a polarizer microscope (ML-9300, Meijitech). The applied voltage and the wavelength of patterns were measured with an electric multimeter (Keithley-2000) and an optical micrometer (Nikon), respectively. In order to capture the change of patterns with real time on a computer, we have used an image soft (Scion Image) and an image board (PCI-VE5, Scion Corporation Company).

We have found typical patterns between crossed polarizers, as shown in Fig. 2. The side-view WD was observed in Fig. 2(a), which corresponds to the well-known WD in the standard top view (in the  $xy$  plane) cells. Due to the small thickness  $r$ , the wavelength of the present WD is much smaller than that of the standard cells ( $\lambda_c \sim d$ ). Above a threshold voltage  $V_c$  microparticles flew along the  $z$  axis, i.e., the orientation of the arrows depicted in the picture. Increasing  $V$  further from  $V_c$ , the WD was evolving into an unexpected pattern in Fig. 2(b). Hereafter we call it the sawteeth pattern (STP). The STP showed a peculiar flow along the

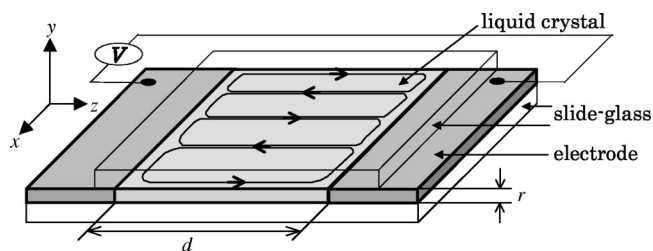


FIG. 1. A Hele-Shaw (side-view) cell. Electroconvection patterns are observed in the  $xz$  plane. In the case of the standard (top-view) cells, one observes the patterns in the  $xy$  plane for  $r \gg d$ . The director of a liquid crystal (MBBA) with a negative dielectric anisotropy ( $\Delta\epsilon < 0$ ) has a preferred orientation along the  $x$  axis. An electric field is applied parallel to the  $z$  axis.

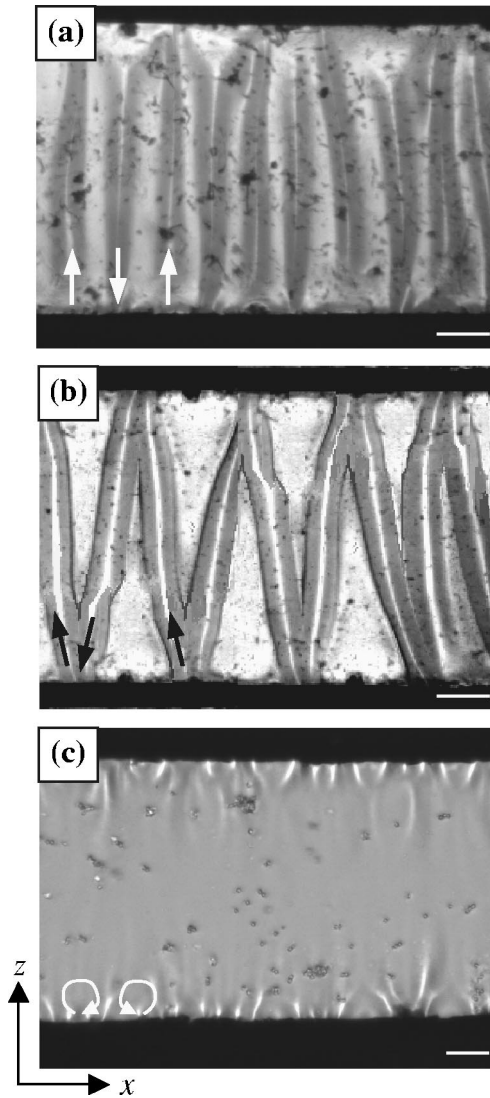


FIG. 2. Typical patterns in a Hele-Shaw cell ( $r=12 \mu\text{m}$ ,  $d=500 \mu\text{m}$ ). (a) The side-view WD (Williams domain at  $V=35 \text{ V}$  and  $f=2000 \text{ Hz}$ ), (b) the sawteeth pattern (STP at  $V=42 \text{ V}$  and  $f=2000 \text{ Hz}$ ), (c) the surface vortices corresponding to the chevron pattern in the standard (top-view) cells (at  $V=130 \text{ V}$  and  $f=6000 \text{ Hz}$ ). The arrows indicate the direction of the flows corresponding to electroconvection. The scale of the white bars is  $100 \mu\text{m}$ .

edges of the sawteeth, as depicted in Fig. 2(b). Figures 3 show an evolution process with increasing  $V$ . The sawteeth start to grow near both the electrodes [see the lower part of Fig. 3(d)], and then they form a remarkable STP [in Fig. 3(e)]. Eventually, at a high voltage it becomes a fully developed turbulence state called the dynamic scattering mode [8,9].

On the other hand, above a critical frequency  $f_c$  a clearly different pattern was found in Fig. 2(c), which may correspond to the so-called chevron pattern found in the standard cells [8,10,13,14]. There exist small-scale vortices near both the electrodes, as can be seen in Fig. 2(c). A surface instability must be dominating in this (dielectric) regime ( $f > f_c$ ). By observing a starting flow, we have determined  $V_c$

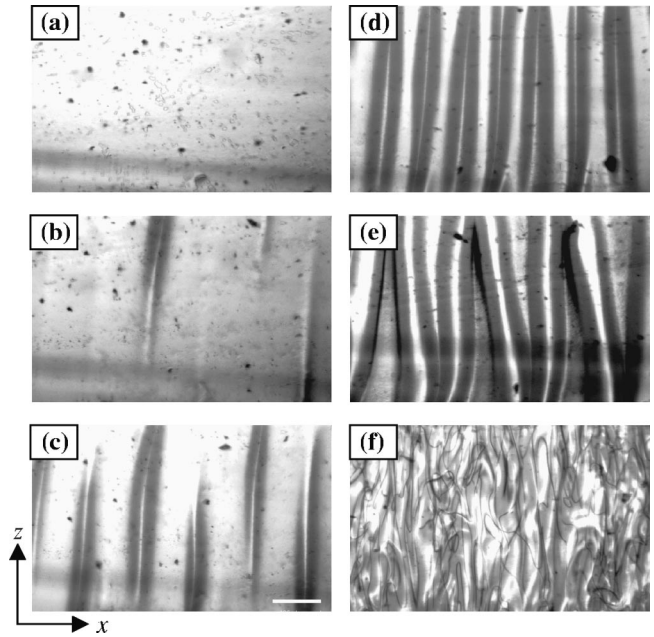


FIG. 3. A pattern evolution with increasing voltage for a fixed frequency  $f=100 \text{ Hz}$  ( $r=12 \mu\text{m}$ ,  $d=1000 \mu\text{m}$ ). (a)  $0 \text{ V}$ , (b)  $42 \text{ V}$ , (c)  $54 \text{ V}$ , (d)  $63 \text{ V}$ , (e)  $73 \text{ V}$ , and (f)  $135 \text{ V}$ . They show a successive transition from a rest state (a) to a fully developed turbulence (f). An unexpected sawteeth pattern (STP) is found in (e). (c) and (f) correspond to WD and the dynamic scattering mode (DSM) observed in the standard (top-view) cells, respectively. The scale of the white bar in (c) is  $200 \mu\text{m}$ .

with changing  $f$ , as shown in Fig. 4. As in the case of the standard cells, we have reproduced the characteristic frequency dependence of  $V_c$  [15] below and above  $f_c$  [1,2,16,17].

We have investigated the stability of the standard convective structure [i.e., the WD in Fig. 2(a)] by the voltage-

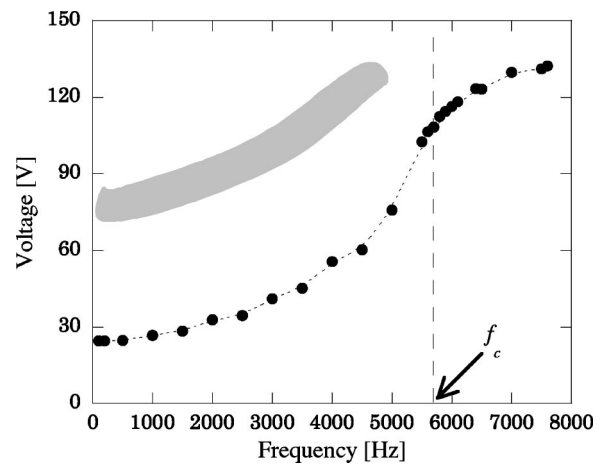


FIG. 4. The frequency-dependence of the threshold voltage  $V_c$  for electroconvection in a Hele-Shaw cell ( $r=12 \mu\text{m}$ ,  $d=1000 \mu\text{m}$ ). The  $f_c$  represents the cutoff frequency ( $f_c \sim 5700 \text{ Hz}$ ). The STPs are found in the shadowed parts above  $V_c$ , where the threshold has not been precisely determined because of inherent experimental difficulties.

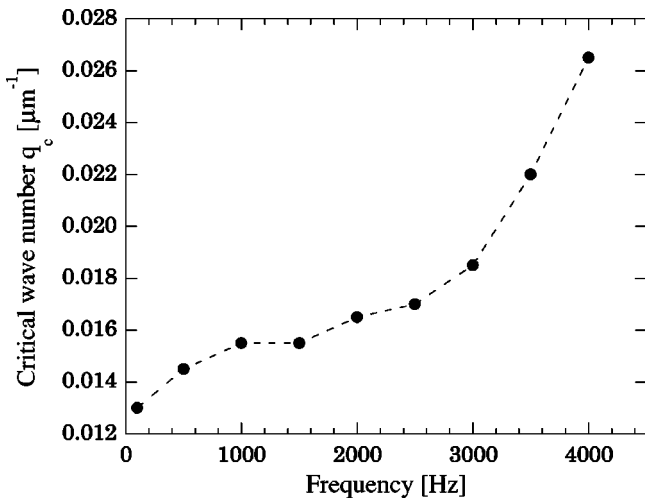


FIG. 5. The critical wave number  $q_c$  of the side-view WD at applied frequencies  $f$  ( $r=12 \mu\text{m}$ ,  $d=1000 \mu\text{m}$ ).  $q_c$  ( $f=f_0=100 \text{ Hz}$ )= $0.013 \mu\text{m}^{-1}$  was chosen for the voltage-frequency jump method (see the detail in the text).

frequency jump method [4,11,18]. In order to determine stable structures, we have measured the critical wave number  $q_c(f)$  at the onset of convection [19], as shown in Fig. 5. We have chosen a final stable structure  $q_c=0.013 \mu\text{m}^{-1}$  at  $V_c=22.5 \text{ V}$  and  $f_0=100 \text{ Hz}$ , to which a jump was made from any initial states with the wave number  $q_i$ . When jumping from the initial states  $q_i(V_i, f_i)$  to the final state  $q_c(V_c, f_0)$  by changing  $V$  and  $f$  simultaneously under the GPIB control of the field generator, we have observed the transient process

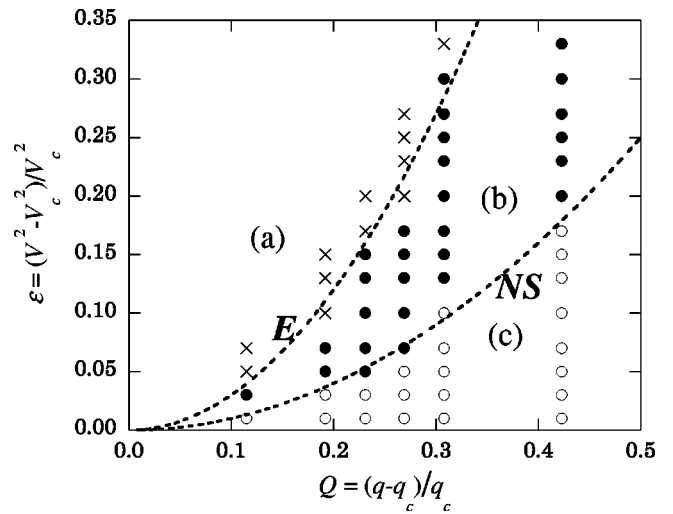


FIG. 6. The Busse diagram in a Hele-Shaw cell ( $r=12 \mu\text{m}$ ,  $d=1000 \mu\text{m}$ ). **E** and **NS** indicate Eckhaus and neutral stability lines, respectively. They are theoretically well known as  $\epsilon_E \sim 3Q^2$  for **E** and  $\epsilon_{NS} \sim Q^2$  for **NS**, as depicted. For (a)–(c), see the corresponding pattern selections after the voltage-frequency jump in Figs. 7 (with same labeling).

of pattern dynamics. Figure 6 shows typical pattern-selection processes in the  $Q-\epsilon$  plane, where  $Q=(q-q_c)/q_c$  and  $\epsilon=(V^2-V_c^2)/V_c^2$  are the normalized wave number and voltage, respectively. In region (a) above **E**-line ( $\epsilon_E \sim 3Q^2$ : Eckhaus line) the pattern with  $q_i$  had no remarkable change, while it experienced the well-known Eckhaus instability in

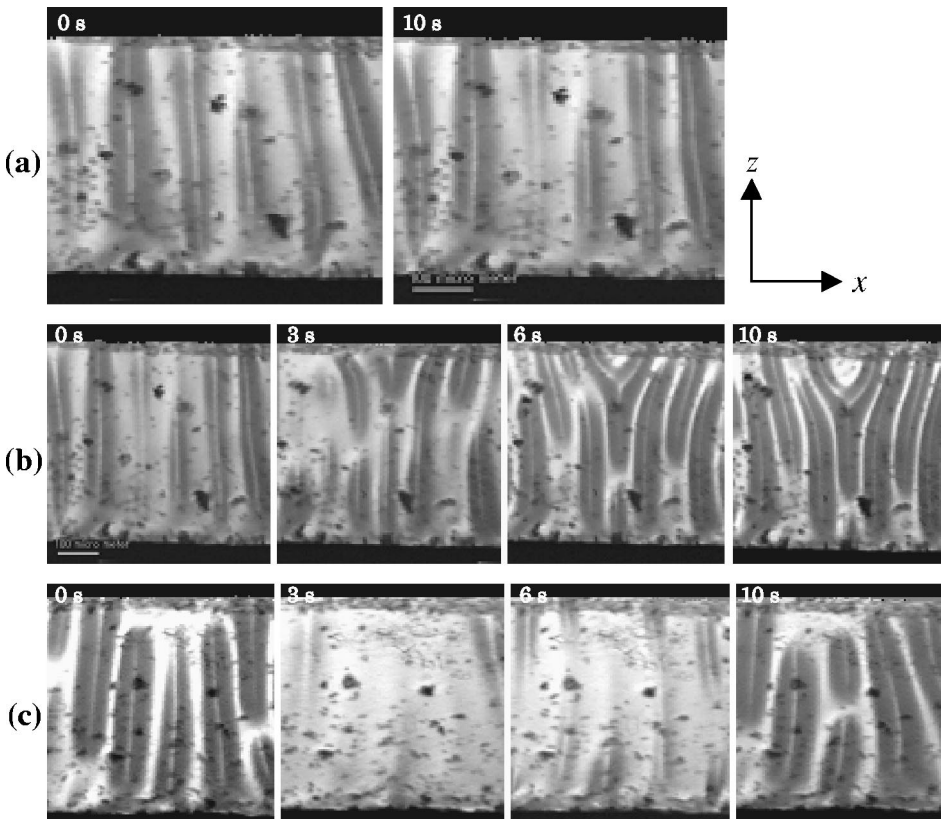


FIG. 7. Pattern selections after the voltage-frequency jump. (a) no remarkable change, (b) the Eckhaus instability, (c) simple decaying and rearranging. These pattern selections arise in regions (a)–(c) in Fig. 6 (with same labeling).

region (b) between **E** lines and **NS** ( $\epsilon_{NS} \sim Q^2$ : neutral stability line) lines. In region (b) we have observed creation and annihilation of the convective structure pairs, as seen in the upper parts of Fig. 7(b). In region (c) the pattern with  $q_i$  decays monotonically and appears again with  $q_c$ . Their corresponding processes are shown in Fig. 7. Although any other instabilities such as zigzag and skewed varicose instability were not found due to the present geometry, we have experimentally observed the neutral and Eckhaus instability boundaries and checked a consistency of the two instability lines in the stability diagram in Hele-Shaw cells [4,13,20,21].

In summary, we have directly observed the convective structures below and above a critical frequency  $f_c$  in Hele-Shaw (side-view) cells. By observing the motion of micro-particles, the convective structures below and above  $f_c$  could be discriminated. The small vortices near both the electrodes were dominating above  $f_c$ , while the large convective structure was manifested below  $f_c$ . Although these surface and/or

bulk instabilities in the dielectric region ( $f > f_c$ ) have been discussed for a long time in the standard (top-view) cells [14,16,17], our experimental results in Hele-Shaw cells obviously support the surface instability. Moreover, compared to the standard cell case a strong anchoring due to the smallness of  $r$  causes a large shift of the threshold voltage and small wavelengths. We have also found an unexpected convective structure (STP) with a peculiar flow that has never been reported in the standard cells, namely, due to the geometric dimension of cells as well as the director alignment, the successive pattern-forming scenario to turbulence is dramatically changed [22,23]. Finally, the universal relationship between Eckhaus and neutral curves in the Busse diagram for quasi-one-dimensional systems has been successfully confirmed in the present Hele-Shaw cells.

We would like to thank S. Suenaga for technical support. This work was partly supported by a Grant-in-Aid for Scientific Research from the Japan Society for the Promotion of Sciences.

- 
- [1] L. Kramer and W. Pesch, *Annu. Rev. Fluid Mech.* **27**, 515 (1995).
- [2] W. Pesch and U. Behn, in *Evolution of Spontaneous Structures in Dissipative Continuous System*, edited by F.H. Busse and S.C. Muller (Springer, New York, 1998).
- [3] E.F. Carr, *Mol. Cryst. Liq. Cryst.* **7**, 256 (1969); W. Helfrich, *J. Chem. Phys.* **51**, 4092 (1969).
- [4] S. Nasuno, O. Sasaki, S. Kai, and W. Zimmermann, *Phys. Rev. A* **46**, 4954 (1992).
- [5] E. Plaut, W. Decker, A.G. Rossberg, L. Kramer, W. Pesch, A. Belaidi, and R. Ribotta, *Phys. Rev. Lett.* **79**, 2367 (1997).
- [6] J.-H. Huh, Y. Hidaka, and S. Kai, *Phys. Rev. E* **58**, 7355 (1998); J.-H. Huh, Y. Hidaka, A.G. Rossberg, and S. Kai, *ibid.* **61**, 2769 (2000).
- [7] H. Richter, A. Buka, and I. Rehberg, *Phys. Rev. E* **51**, 5886 (1995).
- [8] S. Kai, K. Yamaguchi, and K. Hirakawa, *Jpn. J. Appl. Phys.* **14**, 1653 (1975).
- [9] S. Kai, W. Zimmermann, M. Andoh, and N. Chizumi, *Phys. Rev. Lett.* **64**, 1111 (1990).
- [10] M. Scheuring, L. Kramer, and J. Peinke, *Phys. Rev. E* **58**, 2018 (1998).
- [11] E. Braun, S. Rasenat, and V. Steinberg, *Europhys. Lett.* **15**, 597 (1991); M. Lowe, J.P. Gollub, *Phys. Rev. Lett.* **55**, 2575 (1985).
- [12] J.-H. Huh, Y. Yusuf, Y. Hidaka, and S. Kai, *Phys. Rev. E* **66**, 031705 (2002).
- [13] J.-H. Huh, Y. Hidaka, and S. Kai, *Mol. Cryst. Liq. Cryst.* **366**, 2685 (2001).
- [14] H. Bohatsch and R. Stannarius, *Phys. Rev. E* **60**, 5591 (1999).
- [15] Due to the smallness of  $r$ , whole liquid crystals in bulk experience a strong anchoring from the glass substrates. Therefore the director cannot easily rotate by the applied electric field even at the center of both electrodes. In other words, such an anchoring effect to the whole cell induces a large increase of the effective elastic constant for the corresponding deformation mode. This causes a large shift of  $V_c$  from the standard values  $V_c(f)$  ( $\sim 8$  V at  $f=100$  Hz).
- [16] P.G. de Gennes and J. Prost, *The Physics of Liquid Crystals*, 2nd ed. (Oxford University Press, New York, 1993).
- [17] L.M. Blinov and V.G. Chigrinov, *Electrooptic Effects in Liquid Crystalline Materials* (Springer-Verlag, New York, 1994).
- [18] G. Goren, I. Procaccia, S. Rasenat, and V. Steinberg, *Phys. Rev. Lett.* **63**, 1237 (1989).
- [19] In the steady states,  $q_c$  was determined near the threshold  $V_c$ .
- [20] S. Kai, K. Hayashi, and Y. Hidaka, *J. Phys. Chem.* **100**, 19 007 (1996).
- [21] A.G. Rossberg, Ph.D. thesis, University of Bayreuth, 2000 (unpublished).
- [22] A.G. Rossberg, A. Hertrich, L. Kramer, and W. Pesch, *Phys. Rev. Lett.* **76**, 4729 (1996).
- [23] Y. Hidaka, J.-H. Huh, K. Hayashi, S. Kai, and M.I. Tribelsky, *Phys. Rev. E* **56**, R6256 (1997); J.-H. Huh, Y. Hidaka, and S. Kai, *J. Phys. Soc. Jpn.* **68**, 1567 (1999).